Tricritical O(n) models in two dimensions

Bernard Nienhuis,[1] Wenan Guo (郭文安),[2] and Henk W. J. Blöte[3,4]
[1]*Instituut voor Theoretische Fysica, Universiteit van Amsterdam, Valckenierstraat 65, The Netherlands*
[2]*Physics Department, Beijing Normal University, Beijing 100875, China*
[3]*Faculty of Applied Sciences, Delft University of Technology, P.O. Box 5046, 2600 GA Delft, The Netherlands*
[4]*Instituut Lorentz, Leiden University, P.O. Box 9506, 2300 RA Leiden, The Netherlands*
(Received 3 September 2008; published 5 December 2008)

We show that the exactly solved low-temperature branch of the two-dimensional O(n) model is equivalent to an O(n) model with vacancies and a different value of n. We present analytic results for several universal parameters of the latter model, which is identified as a tricritical point. These results apply to the range $n \leqslant 3/2$ and include the exact tricritical point, the conformal anomaly, and a number of scaling dimensions, among which are the thermal and magnetic exponents, and the exponent associated with the crossover to ordinary critical behavior and to tricritical behavior with cubic symmetry. We describe the translation of the tricritical model in a Coulomb gas. The results are verified numerically by means of transfer-matrix calculations. We use a generalized ADE model as an intermediary and present the expression of the one-point distribution function in that language. The analytic calculations are done both for the square and the honeycomb lattice.

DOI: 10.1103/PhysRevE.78.061104 PACS number(s): 05.50.+q, 64.60.Cn, 75.10.Hk

I. INTRODUCTION

The O(n) model is defined in terms of n-component spins on a lattice that interact in an isotropic way. Graph expansion [1] of the partition integral of this model leads to a weighted sum of graphs, in which every node is connected to its neighbors by an even number of bonds. In the resulting partition sum, the spin dimensionality n is only a parameter and may be varied continuously. For a special choice of the model on the honeycomb lattice, one thus derives a model of nonintersecting loops [2]. Exact results for the universal parameters [3] as a function of n were obtained for this O(n) model for two cases, one of them describing the critical point and the other a special (see [4]) case of the low-temperature phase. These results are described in the context of the Coulomb gas in a review by Nienhuis [5].

These two cases of universal behavior were also found along two branches of a square-lattice O(n) model [6,7], together with two different branches describing the critical behavior that occurs when O(n) and Ising degrees of freedom on the square lattice display a joint critical point. But it took a long time before an exact description was also proposed [8] for the *tricritical* O(n) universal parameters in two dimensions as a function of n. The plausibility of this description follows from earlier identifications of the fully packed O(n) loop model with the critical Potts model and of the critical O(n) model with the tricritical Potts model [3]. Therefore it seemed plausible that the tricritical O(n) model is associated with an even higher critical Potts model. Such a model is known in the form of the tri-tricritical Potts model, for which some universal parameters are known [9,10]. Moreover, these universal parameters were found to agree accurately with numerical estimates of the conformal anomaly and some critical exponents of the tricritical O(n) model on the honeycomb lattice.

In this paper we provide a more exact basis for this characterization of the tricritical O(n) universal parameters by means of an exact mapping between an O(n)-symmetric spin model with vacancies and an O(n') loop model without vacancies which was exactly solved in Refs. [6,11]. This mapping consists of several steps. One of these maps the spin model with vacancies onto a loop model with vacancies, as reported in Sec. II. It includes, as a limiting case, the mapping between both models without vacancies. In Sec. III, we first represent the exactly solved square-lattice loop model [6,11] as a generalized ADE model involving discrete site variables, separated by domain walls. Some of the states of these site variables are interpreted as vacancies. Then, summation over the remaining states leads to an O(n) loop model with vacancies and with a modified loop weight n. The latter model can again be transformed into an O(n) spin model with vacancies and with a number n of spin components different from that of the spin representation of the original loop model without vacancies. Section III also provides a similar analysis involving models on the honeycomb lattice and the interpretation of the models with vacancies as tricritical models. We include a mapping on the Coulomb gas, which yields some critical exponents, including the one that is responsible for a crossover to models with cubic symmetry. This part is presented in Sec. IV. In Sec. V we define the transfer matrix and apply it to confirm numerically some of the predicted exponents. Results and consequences are discussed in Sec. VI.

II. MAPPING OF THE SPIN MODEL ON A SOLVABLE LOOP MODEL

As a candidate system to display O(n) tricriticality, we choose a generalized version of the $O(n)$ spin model on the square lattice studied by Nienhuis and co-workers [6,7,11]. The n-component spins occupy the midpoints of the lattice edges. They are denoted $\vec{s}_i$ where the index i labels the corresponding edge. The integration measure is normalized by $\int d\vec{s}=1$ and the mean length of the spins by $\int d\vec{s}(\vec{s}\cdot\vec{s})=n$. The

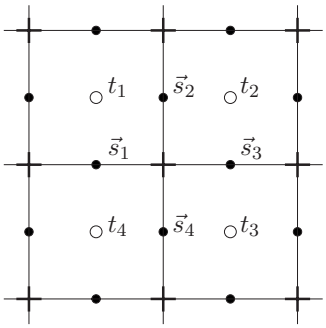

FIG. 1. Part of the square lattice with spin variables (●) and face variables (○) representing the vacancies. The vertices are shown as +. The figure includes the labeling of the variables used in the definition of the local weight $W(k)$, when applied to the central vertex in this figure.

distribution is chosen isotropic—i.e., in accordance with O(n) symmetry. The model also includes face variables $t_j=0$ or 1, which sit on the faces of the square lattice. The index j labels the corresponding face. The value $t_j=0$ corresponds to a "vacancy" which has the effect of eliminating the interactions involving any of the four adjacent spins. The vacancies thus introduce dilution and may thus be expected to lead to a tricritical transition, analogous to that in the Potts model.

We write the partition sum as

$$Z_{\text{spin}} = \left[\prod_{\text{faces } j} \sum_{t_j=0}^{1}\right]\left[\prod_{\text{edges } i} \int d\vec{s}_i\right] \prod_{\text{vert } k} W(k). \tag{1}$$

While the spins reside on the edges of the lattice and the vacancies on the faces, the Boltzmann weight factorizes into factors $W(k)$ giving the interaction between all variables incident on a vertex. A part of the lattice is shown in Fig. 1. The local weight $W(k)$ is defined by

$$\begin{aligned} W(k) \equiv \Bigg\{ & 1 + u\sum_{i=1}^{4} [(p + (1-p)t_{i+2})t_i t_{i+1} t_{i+3} \vec{s}_i \cdot \vec{s}_{i+1}] \\ & + t_1 t_2 t_3 t_4 \sum_{i=1}^{2} [v\vec{s}_i \cdot \vec{s}_{i+2} + w(\vec{s}_i \cdot \vec{s}_{i+1}) \\ & \times (\vec{s}_{i+2} \cdot \vec{s}_{i+3})] \Bigg\} V(t_1,t_2,t_3,t_4), \end{aligned} \tag{2}$$

where the indices of the $\vec{s}$ and t variables are defined modulo 4. They describe the position of the variables in the local configuration as specified in Fig. 1 around the vertex k. The vacancy weight $V(t_1,t_2,t_3,t_4)$ per vertex is specified by

$$\begin{aligned} V(t_1,t_2,t_3,t_4) \equiv & \ \delta_{t_1+t_2+t_3+t_4,4} + v_1 \delta_{t_1+t_2+t_3+t_4,3} \\ & + v_2 \delta_{t_1+t_2+t_3+t_4,2} \delta_{t_1,t_3} + v\, \delta_{t_1+t_2+t_3+t_4,2}(1-\delta_{t_1,t_3}) \\ & + v_3 \delta_{t_1+t_2+t_3+t_4,1} + v_4 \delta_{t_1+t_2+t_3+t_4,0}, \end{aligned} \tag{3}$$

so that the index of v_i indicates the number of vacancies. The expansion in loop diagrams proceeds analogous to Ref. [7], but as a consequence of the added t variables, the loops are restricted to the edges that are not adjacent to a vacancy. Furthermore, the term $p(1-t_{i+2})$ leads to an additional potential for a loop segment that, with respect to a vertex, is diagonally opposite to a vacancy. The loop expansion transforms the partition function into

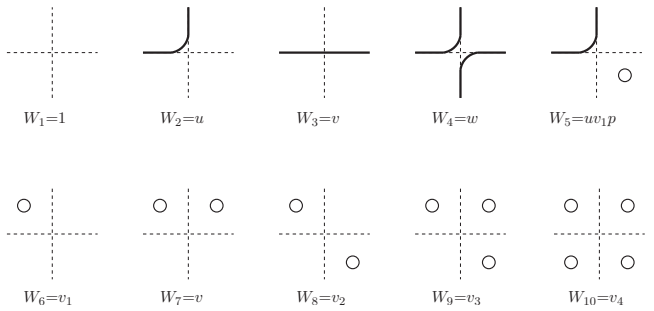

FIG. 2. Vertex weights of the O(n) model with vacancies. The solid lines represent loop segments and the open circles the vacancies on the faces of the lattice. The presence of a vacancy implies that the four surrounding edges are not visited by a loop. The absence of a circle corresponds to an occupied face, whose edges may or may not be visited by a loop. The same weights apply to rotated versions of the vertices shown here. The spin variables, which sit on the middle of the edges, are absent in the loop representation.

$$Z_{\text{spin}} = Z_{\text{loop}} = \left[\prod_{j} \sum_{t_j=0}^{1}\right] \sum_{\{\mathcal{L}\}|\{t\}} n^{N_{\text{L}}} \prod_{i=1}^{10} W_i^{N_i}, \tag{4}$$

where the second sum is on all configurations $\mathcal{L}$ of closed loops, covering zero or more edges of the square lattice, while avoiding edges adjacent to a vacancy. Every vertex is of one of ten types shown in Fig. 2. The total number of vertices of type i is denoted N_i and the total number of loops as N_{L}. The vertex weights W_i are given in Fig. 2 in terms of the parameters that already appear in the spin representation of Eq. (2).

III. EXACT ANALYSIS

A. Dense loop model

Consider the exactly solved low-temperature branch of the O(n) loop model on the square lattice, named branch 2 in [7,6]. Its partition sum, although of the form of Eq. (4), is denoted $Z_{\text{dense loop}}$, referring to the relatively dense filling of the lattice with loops. The weights can be parametrized in terms of the angle $\theta \in [0, \pi/2]$. As a consequence of the absence of vacancies, only the vertices labeled 1–4 in Fig. 2 have nonzero weight; their weights are specified as

$$\begin{aligned} W_2 &= u = h(\theta)\sin(\theta), \\ W_3 &= v = h(\theta)\sin(3\theta/4), \\ W_4 &= w = h(\theta)\sin(\theta/4), \end{aligned} \tag{5}$$

with $h(\theta) \equiv 1/[2\sin(\theta)\cos(3\theta/4) + \sin(3\theta/4)]$. The weight of the loops (or the dimensionality of the spins) is

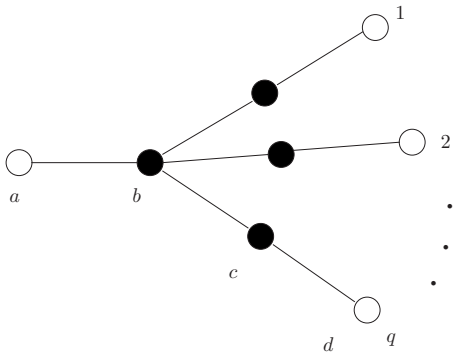

FIG. 3. The adjacency diagram $\mathcal{A}$ having q branches. For $q=0$, 1, and 2, it reduces to the diagrams A_2, A_4, and E_6, respectively.

$$n' = -2\cos(2\theta). \tag{6}$$

We use n' because we wish to reserve n for another model that will appear later, in which all weights W_k are nonzero.

B. ADE models

Here we construct an alternative representation of the loop model partition sum. Following Pasquier [12,13], the loops are interpreted as domain walls in a configuration of discrete variables residing on the faces of the lattice. These variables take values corresponding to the nodes of a graph $\mathcal{A}$ called the adjacency diagram. In this paper we consider the family of graphs shown in Fig. 3, but the discussion in this section is general and the figure can be seen as an example. We call this model an ADE model after the classification of adjacency diagrams. Neighboring faces not separated by a loop carry the same value. If they are separated by a loop, their values are *adjacent* in $\mathcal{A}$ (hence its name).

Associated with $\mathcal{A}$ we introduce the adjacency matrix $\mathbf{A}$ with elements $A_{i,j}$, where i and j represent nodes of $\mathcal{A}$. The elements are defined as $A_{i,j}=1$ if i and j are adjacent and $A_{i,j}=0$ otherwise. Of the $2(1+q)$ eigenvectors of $\mathbf{A}$, four are symmetric under permutation of the q branches. In the symmetric subspace the eigenvector equation can be written as that for the right-hand eigenvector of the 4×4 matrix $\tilde{A}_{i,j}$:

$$\tilde{\mathbf{A}} = \begin{pmatrix} 0 & 1 & 0 & 0 \\ 1 & 0 & q & 0 \\ 0 & 1 & 0 & 1 \\ 0 & 0 & 1 & 0 \end{pmatrix}. \tag{7}$$

The first two elements of the eigenvectors of $\tilde{\mathbf{A}}$ correspond to the nodes a and b, respectively, and the last two with the nodes of type c and d, respectively (see Fig. 3). We choose the number of branches of the diagram $\mathcal{A}$ to be $q=(n'-1/n')^2$, so that the symmetric eigenvalues Δ_μ of $\tilde{\mathbf{A}}$ are given by

$$\Delta_0 = n',$$

$$\Delta_1 = 1/n',$$

$$\Delta_2 = -1/n',$$

$$\Delta_3 = -n', \tag{8}$$

and for each of these eigenvalues, the elements of the corresponding eigenvectors are

$$(S_a^\mu, S_b^\mu, S_c^\mu, S_d^\mu) = (\Delta_\mu - 1/\Delta_\mu, \Delta_\mu(\Delta_\mu - 1/\Delta_\mu), \Delta_\mu, 1). \tag{9}$$

Besides these, there are $2(q-1)$ eigenvectors antisymmetric for interchange of two of the branches of $\mathcal{A}$. They have eigenvalues

$$\Delta_4 = 1,$$

$$\Delta_5 = -1, \tag{10}$$

each $(q-1)$-fold degenerate.

Of the eigenvectors of $\mathbf{A}$, generally denoted as S_j^μ, we omit the upper index for the case $\mu=0$. For $n'>1$ this is the Perron-Frobenius eigenvector, with eigenvalue $\Delta_0=n'>\Delta_\mu$ for $\mu=1,2,3$.

We write the weight of the corresponding ADE model in terms of a product of local weight factors as

$$W_{\mathrm{ADE}} = \prod_{\mathrm{vert}k} W(k) \prod_{\mathrm{turns}} A_{i,j} \left(\frac{S_i}{S_j}\right)^{\gamma_{\mathrm{bend}}/2\pi}. \tag{11}$$

There is a factor $W(k)$ for each vertex depending only on the local configuration of domain walls and a factor for each turn of the domain wall which also depends on the states of the faces on the inside (i) and outside (j) of the loop. The bending angles γ_{bend} are counted positive where the loop bends inwards, so that the sum of the bending angles along a loop is $+2\pi$. Thus the weight of an entire closed domain wall is

$$W_{\mathrm{loop}} = A_{i,j}\frac{S_i}{S_j} \tag{12}$$

and still depends on the state i inside and j outside the domain wall. When for a fixed configuration of domain walls the sum over compatible state configurations is performed, each closed domain wall thus contributes a factor equal to the largest eigenvalue of $\mathbf{A}$—i.e., n'—just as in the O(n') loop model. This confirms that the partition function of the ADE model satisfies

$$Z_{\mathrm{ADE}} \equiv \sum_{\mathcal{G}} \sum_{\{s\}|\mathcal{G}} W_{\mathrm{ADE}} = Z_{\mathrm{dense\ loop}}, \tag{13}$$

where the first sum is on all loop configurations and the second one on the configurations of ADE variables compatible with the loops. The suffix of the right-hand side emphasizes that the loop model is in the dense phase and does not permit vacancies, which will be introduced later. Since in $Z_{\mathrm{dense\ loop}}$ the variable n' and therefore q only enter as parameters, we may vary them continuously, thus representing the continuous n'-weight loop model.

When the models reside on a torus rather than in the plane, there may be loops that wind the torus. In the loop model these typically have the same weight n' as the contractible loops. However, in the ADE model, the corresponding domain walls have a net bending angle equal to zero. This implies that they carry the weight $A_{j,k}$ rather than $A_{j,k}S_j/S_k$. The summation over the states of the domains then

reduces to taking the trace of a power of **A**, equal to the number of noncontractible loops. The result is that all the winding loops have the same weight, equal to an eigenvalue of **A**, which should then be summed over these eigenvalues. We conclude that the ADE model on a torus corresponds to a loop model in which the winding loops receive special treatment. Or alternatively the loop model partition sum with all loops weighted equally is the largest sector of the ADE transfer matrix.

C. Correlation functions

We will now calculate the one-point distribution (1PD) $P(k)$ of the ADE model—i.e., the probability that a face is in state k. Consider a loop well inside a large lattice. We assume that the 1PD is unaffected by the presence of the loop (or any other loop). In other words, we assume that the 1PD conditional on the presence of a loop is the same as the unconditional 1PD. That this is plausible follows from the calculation of the partition sum above: the contribution to the partition sum of a particular domain is independent of the domains it is contained in, and it is independent of all the domains it contains, once the state of these domains has been summed over.

The conditional probability $P(k|j)$ that the inside domain of a loop is in state k, provided the outside domain is in a given state j, is determined by Eq. (12) as $P(k|j) = A_{k,j}S_k/(n'S_j)$. Thus we find the joint probability $P(k,j)$ that the outside of a loop is in state j *and* its inside in state k as

$$P(k,j) = P(j)P(k|j) = P(j)A_{k,j}\frac{S_k}{n'S_j}. \tag{14}$$

Summation on j now yields the probability that the inside domain is in state k, which should be equal to $P(k)$:

$$\sum_j P(k,j) = P(k). \tag{15}$$

Using the symmetry of **A**, one finds the unique (normalized) solution to this consistency condition as

$$P(k) = \frac{S_k^2}{\Sigma_j(S_j^2)}. \tag{16}$$

An approach alternative to the condition that the loop considered be well inside a large lattice is to consider a bounded lattice of arbitrary size, with the faces on the boundary all in the same state, with Eq. (16) as the probability distribution for that state, the ideal fixed boundary condition. Then by induction the same distribution holds for the domains separated from the boundary by one domain wall and so on recursively to the innermost domains. It is then assumed that in the thermodynamic limit the boundary condition should not matter, well away from the boundary.

Consider the function S_k^μ/S_k—i.e., the ratio of an arbitrary eigenvector S^μ and the Perron-Frobenius eigenvector S. If this function is part of a correlation function $\langle \cdots S_k^\mu/S_k \cdots \rangle$, where k is the state of a given face, it effectively changes the weight of the loops *surrounding the face*. This is easily seen in expression (12): the factor S_k^μ/S_k replaces the numerator by S_k^μ, so that the weight of the loop becomes that of the corresponding eigenvalue Δ_μ, as long as they do not surround other operator insertions. We will call these functions weight-changing operators.

A more interesting result [14] comes from the two-point function

$$\left\langle \frac{S_j^\mu}{S_j}\frac{S_k^\nu}{S_k} \right\rangle, \tag{17}$$

j and k being the state of two arbitrary faces. The weights of the loops surrounding either of these faces but not the other is changed into the respective eigenvalues Δ_μ and Δ_ν, corresponding to the eigenvectors S^μ and S^ν. Now consider the innermost domain wall that surrounds both faces. After the states of the domains nested inside it are summed over, the weight governing the state of the final domain is

$$\frac{S_j^\mu S_j^\nu}{S_j^2}A_{j,k}, \tag{18}$$

where k is the state of the surrounding domain. This can be expanded as a linear combination of all eigenvectors:

$$S_j^\mu S_j^\nu = S_j \sum_\kappa C_{\mu\nu}^\kappa S_j^\kappa, \tag{19}$$

where, provided the eigenvectors are normalized,

$$C_{\mu\nu}^\kappa = \sum_j \frac{S_j^\mu S_j^\nu S_j^\kappa}{S_j}. \tag{20}$$

Apparently the combination of two operators labeled μ and ν look from a distance like a linear combination of operators κ.

These structure constants of the operator product expansion, or fusion rules, may readily be calculated explicitly for the diagrams in Fig. 3, but here we only note that they are symmetric in μ, ν, and κ and that they vanish if one of the indices corresponds with the largest eigenvalue and the others two differ. This implies that the two-point correlation function of two different weight-changing operators vanishes in the thermodynamic limit. Obviously these fusion rules may be used just as well in correlation functions of more than two operators.

D. Equivalence with the O(n) model with vacancies

We now dilute the system by considering the extremal nodes of $\mathcal{A}$—i.e., the nodes with coordination number 1—as vacant states. The obvious result is that vertices with vacancies, numbered 5,…,10, will have nonzero weight. The present subsection will also yield the less obvious result that the model with vacancies can still be expressed as an O(n) model, now with a different value of n.

The vacancies come in $q+1$ types, q of type d and one a. However, in any configuration the type of each vacancy is fully determined by the neighboring domains. Thus, it is sufficient to specify the $q+1$ states for the nonvacant domains in order to fully describe an ADE configuration (with the exception of the completely vacant state).

Now we identify the domain walls between domains in state b and in states of type c as loops, so that we have a loop model with vacant faces. Note that for any given configuration of vacancies this loop model is much like that described in Sec. III B, but on a restricted lattice, from which the vacant faces are omitted, and with a reduced adjacency diagram, of only the full nodes in Fig. 3. Note that the eigenvectors of the reduced adjacency matrix, up to normalization, are the same as the eigenvectors of the total adjacency matrix, restricted to the nodes b and those of type c. The eigenvalues are $\pm\sqrt{q}$. Following the arguments used before, we obtain a loop model with loop weight $n=\sqrt{q}=n'-1/n'$, with weights that follow from the original ADE model with the complete adjacency diagram and the entire lattice. Thus the successive transformations are

$$Z_{\text{dense loop}} \to Z_{\text{ADE}} \to Z_{\text{loop+vac}}, \tag{21}$$

in which the right-hand side is the partition sum of a model with loops and vacancies. The weights of this loop model are, with reference to Fig. 2, given by

$$W_1 = 1,$$

$$W_2 = u,$$

$$W_3 = v,$$

$$W_4 = w,$$

$$W_5 = w(S_a/S_b)^{1/4} = w(S_d/S_c)^{1/4} = w(n')^{-1/4},$$

$$W_6 = u(S_a/S_b)^{1/4} = u(S_d/S_c)^{1/4} = u(n')^{-1/4},$$

$$W_7 = v,$$

$$W_8 = w[(S_a/S_b)^{1/2} + (S_b/S_a)^{1/2}] = w[(S_d/S_c)^{1/2} + (S_c/S_d)^{1/2}] = w[(n')^{-1/2} + (n')^{1/2}],$$

$$W_9 = u(S_b/S_a)^{1/4} = u(S_c/S_d)^{1/4} = u(n')^{1/4},$$

$$W_{10} = 1, \tag{22}$$

respectively. The two terms in W_8 arise from the two orientations of the type-4 vertex of the O(n') loop model.

We note that the weights are completely given by the configuration of loops and vacancies, irrespective of the type of vacancy. Furthermore, any configuration of loops and vacancies consisting of the local vertices in Fig. 2 is possible for the adjacency diagram in Fig. 3. These properties are not generic for any adjacency diagram and are the basis of our choice of the diagram in Fig. 3, together with the fact that is contains a continuously variable parameter controlling the eigenvalues of its adjacency matrix.

E. O(n) model on the honeycomb lattice

A similar O(n) spin model with vacancies on the faces can be defined on the honeycomb lattice; see, e.g., Ref. [8].

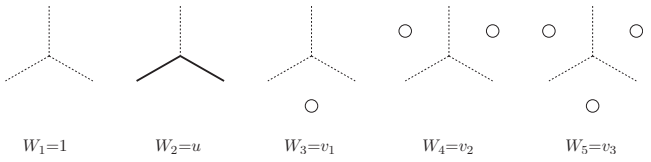

FIG. 4. Vertex weights of the honeycomb O(n) model with vacancies on the faces. Solid lines represent loop segments and circles the vacancies on the elementary hexagons. A vacancy excludes the six surrounding edges to be visited by a loop. Rotated versions of these vertices have the same weights. The spin variables, which sit on the vertices, play no part in the loop representation.

Here we also include interactions between the vacancies, described by the three vertex weights v_1, v_2, and v_3 where the indices show the number of vacancies adjacent to the vertex.

The transformation into a loop model partition sum proceeds the same as for the square lattice and leads to the form of Eq. (4) but with only five independent vertices. They are shown in Fig. 4, together with their weights. For the simplified case $v_1=v_2=v_3=0$ without vacancies and with the special choice [15]

$$u = 1/\sqrt{2 \pm \sqrt{2-n'}} \tag{23}$$

(which is different from that for the square lattice), this model is solvable [15–17]. The high-loop-density branch of this model corresponds to the minus sign.

The mapping of the low-temperature O(n') model on the dilute O(n) model can be performed analogously for the honeycomb lattice and leads to the following vertex weights for the model with vacancies:

$$W_1 = 1,$$

$$W_2 = u,$$

$$W_3 = u(S_a/S_b)^{1/6} = u(S_d/S_c)^{1/6} = u(n')^{-1/6},$$

$$W_4 = u(S_b/S_a)^{1/6} = u(S_c/S_d)^{1/6} = u(n')^{1/6},$$

$$W_5 = 1.$$

The adjacency matrix and thus its eigenvector components are the same as for the square lattice model, Eq. (9). Also the loop weight

$$n = n' - \frac{1}{n'} \tag{24}$$

is the same.

F. Interpretation

It remains to be shown that the constructed model of loops and vacancies is a tricritical O(n) model. To this purpose we obtain its conformal anomaly c via the equivalence with the low-temperature O(n) model of Eq. (5), for which [6,7]

$$c = 1 - \frac{6(1-g)^2}{g}, \quad 2\cos(\pi g) = -n', \quad 0 \leqslant g \leqslant 1, \tag{25}$$

$$n = n' - \frac{1}{n'}.$$

This combination of c and n does not agree with the known critical and low-temperature O(n) universality classes [3]. Since it is known that the introduction of vacancies can lead to tricriticality, this already suggests that the model defined by Eqs. (4), (22), and (24) is tricritical. Further justification will be given below.

IV. UNIVERSAL PROPERTIES AND MAPPING ON THE COULOMB GAS

A. Conformal anomaly

Equation (25) shows that the model with vacancies derived above does not fit the critical and low-temperature O(n) universality classes [3]. It does, however, precisely match the result for c inferred in Ref. [8] for the tricritical O(n) model—namely,

$$c = 1 - \frac{6}{m(m+1)}, \quad 2\cos\frac{\pi}{m+1} = \Delta, \quad m \geqslant 1, \quad n = \Delta - \frac{1}{\Delta}. \tag{26}$$

The parametrizations of n in Eqs. (25) and (26) imply that $n' = \Delta$. This provides a confirmation that the O(n) loop model defined by the vertex weights of Eq. (22) and the loop weight of Eq. (24) is a tricritical O(n) model. For the Ising model $n=1$ and the self-avoiding walk $n=0$, this proposal reproduces the known tricritical values of $c=7/10$ and $c=0$, respectively.

B. Relation with the Coulomb gas

The Coulomb gas offers a powerful tool to calculate critical exponents, provided the Coulomb gas coupling constant g is known for the model under investigation. The coupling constant is related [18,19] to the conformal anomaly c according to Eq. (25). In combination with Eq. (26) this yields g as a function of m, which is two valued. For the tricritical O(n) model one has $g=m/(m+1)$, in agreement with the conformal classification of the tricritical Ising ($n=1$) model. In Coulomb gas language, the conformal anomaly is represented by means of a pair of electric charges e_0 as follows:

$$c = 1 - \frac{6e_0^2}{g}, \quad e_0 = 1 - g, \quad n' = -2\cos\pi g. \tag{27}$$

Combination with another pair of charges $\pm e_\mu$ yields a scaling dimension

$$X_j = \frac{e_\mu^2 - e_0^2}{2g}, \tag{28}$$

which reproduces the dimensions listed in Refs. [8,9] for the tricritical O(n) universality class for charges e_μ according to [5]

$$\cos(\pi e_\mu) = \frac{\Delta_\mu}{2}. \tag{29}$$

The Δ_μ follow from the eigenvalues of the adjacency matrix [12,13], which is the same as that used for the tri-tricritical Potts model [9]. Six eigenvalues were already listed in Ref. [9] and in Eqs. (8) and (10). The leading scaling dimensions follow as

$$X_1 = \frac{(1-t)^2 - (1-g)^2}{2g},$$

$$X_2 = \frac{t^2 - (1-g)^2}{2g},$$

$$X_3 = 1 - \frac{1}{2g},$$

$$X_4 = 1 - \frac{4}{9g} - \frac{g}{2},$$

$$X_5 = 1 - \frac{5}{18g} - \frac{g}{2}, \tag{30}$$

with

$$t = \frac{1}{\pi}\arccos\frac{1}{2\cos(\pi g)}. \tag{31}$$

These exponents are associated with the weight-changing operators S_k^μ / S_k, discussed in Sec. III C. This implies [see Eq. (9)] that the X_2 is associated with the enhancement (or suppression) of vacancies: its eigenvector has a different signs in the vacant and nonvacant states. It follows that X_2 is one of the thermal exponents, leading or otherwise. The exponent X_1 belongs to the operator that breaks the pseudosymmetry between the left- and right-hand sides of $\mathcal{A}$. It changes the weight of the loops from n to $-n$, but is not meaningful in the local O(n) spin version of the loop model. One can arrange this effect, however, by an operator that terminates a seam across which the interactions have the opposite sign. It will appear later as the interface exponent. The exponent X_3 combines the effect of the prior two operators. Finally the operator associated with the exponent X_4 breaks the symmetry between the q branches, while that of X_5 combines this with the enhancement of vacancies. Again, these operators only show up in models where the nodes of $\mathcal{A}$ are meaningful. In our O(n) models, the diagram is only used to give the proper weights to various configurations.

In addition to the dimensions describing singularities associated directly with the ADE model, we consider exponents describing crossover phenomena due to a possible perturbation of the O(n) symmetry. Such perturbations can, in Coulomb gas language, be associated with pair of electric charges $1-g$ combined with a pair of magnetic charges whose magnitude depends on the type of perturbation [5]. A pair of magnetic charges $\pm k$, associated with the defect of $2k$ lines coming together, then corresponds with a scaling dimension

$$X_{p,k} = 1 - \frac{1}{2g} + \frac{g(k^2-1)}{2}. \tag{32}$$

C. Specific exponents

1. Magnetic exponent

In the O(n) loop model, the magnetic correlation function is represented by configurations containing a single loop segment connecting the correlated points. In Coulomb gas language it corresponds to a magnetic charge $k=1/2$. Then, Eq. (32) yields

$$X_h = 1 - \frac{1}{2g} - \frac{3g}{8}. \tag{33}$$

This is in agreement with an earlier conjecture [20] and with numerical results for a related model with vacancies on the honeycomb lattice [8]. After the mapping onto the model with vacancies, the defects—i.e., the end points of the loop segment—can only sit on nonvacant sites and not in the regions occupied by vacancies. But otherwise, the defects have the same physical effect and, therefore, the same exponent (33). Therefore the magnetic exponent of the tricritical O(n) model is the same as that of the low-temperature O(n') model.

2. Temperature exponent

Above we already identified the exponent X_2 as a thermal exponent. This agrees with identification on the basis of numerical evidence, in [8], as, in fact, the leading thermal exponent. Effects described by this exponent are absent in the thermal properties of the low-temperature O(n') model. This fits well in the interpretation [3] that the latter model is confined to the critical subspace of a larger parameter space. Such "unphysical" O(n') exponents are, however, known to reappear in correlations on dilute O(n) loop configurations [21]. We further remark that the thermal exponent of the O(n') model, associated with the suppression and enhancement of loops, should be another thermal exponent; its value, $4/g-2$, however, indicates that it is irrelevant. Another option to find a second thermal exponent comes from the observation that the value of t in Eq. (31) is only the smallest solution of the inverse cosine. The next leading exponent is obtained by replacing t by $2-t$ in X_2, so that

$$X_2 \to X_{t2} = \frac{(2-t)^2 - (1-g)^2}{2g}. \tag{34}$$

3. Other exponents

The introduction of a "seam"—i.e., a row of antiferromagnetic bonds, such that the bonds are perpendicular to the row—leads to a change of the partition sum described by an "interface" dimension X_m. While in Ref. [8] the identification $X_m=X_1$ was made on the basis of numerical evidence, here we can make the identification by inspection of the corresponding operator. A seam along the length of the cylinder changes the sign of the noncontractible loops. That corresponds precisely to $\Delta_1=1/n'$ in Eq. (8) because inversion of n' results in a change of sign of n.

In the O(n) spin model, other interface exponents can be constructed by the introduction of a cut across which the spin $\vec{s}$ is identified with $\mathbf{R}\cdot\vec{s}$, where $\mathbf{R}$ is an operator in the orthogonal group O(n). The weight of the loops crossing this cut is then equal to $\int d\vec{s}(\vec{s}\cdot\mathbf{R}\cdot\vec{s})$. By varying $\mathbf{R}$ this can take any value. The corresponding exponent is obtained by the relation $\Delta-1/\Delta=\int d\vec{s}\vec{s}\cdot\mathbf{R}\cdot\vec{s}$ and Eqs. (28) and (29).

A cubic perturbation of the O(n) symmetry can be represented by magnetic charges $k=\pm 2$ in Eq. (32) [3,22], which yields

$$X_{p,2} = 1 - \frac{1}{2g} + \frac{3g}{2}. \tag{35}$$

It is the exponent that describes the crossover when a cubic symmetry breaking is introduced. Also when intersections between the loops are permitted, this exponent governs the crossover to another universality class. This indicates the fact that the results in this paper are applicable exclusively when intersections are prevented, by the specific choice of the Hamiltonian.

V. NUMERICAL VERIFICATION

For the construction of the transfer matrix we choose the usual geometry of a model wrapped on a cylinder, such that one of the lattice edge directions runs parallel to the axis of the cylinder. The transfer-matrix method used here is based on that of Ref. [7], including the sparse-matrix composition. The main modification is the generalization of the set of connectivities used in Ref. [7] to include the specification of the vacancy variables on the faces.

A. Enumeration of the connectivities

We consider the model of Eq. (4) on a cylinder with a circumference of L lattice units. The cylinder is has an open end such that there are L external edges, which may or may not be covered by segments of incomplete loops. The connectivity specifies the following information: (a) which of the faces at the end of the cylinder carry vacancies and (b) the way in which pairs of covered external edges are connected by incomplete loops of $\mathcal{L}$. These connectivities are subject to the restriction that the loop segments cannot be adjacent to a vacancy. Each connectivity can be fully specified by a row of integers $(i_1,i_2,\ldots,i_L)$ such that

$i_l=i_m>0$	if and only if edge l is connected to edge m,
$i_k=0$	if and only if edge k is not visited by a loop segment and the face to the right of k is occupied,
$i_n=-1$	if and only if face to the right is vacant.

The positions of the vacancies can simply be coded by means of an L-bit binary number $(p_1,p_2,\ldots,p_L)$ with value $\beta=\Sigma_{k=1}^{L} p_k 2^{k-1}+1$. For a given β, we no longer need those i_k that sit adjacent to a vacancy. After dropping these i_k from $(i_1,i_2,\ldots,i_L)$, let $(j_1,j_2,\ldots,j_u)$ denote the remaining se-

TABLE I. Conformal anomaly c and interface critical dimension X_m as determined from the transfer-matrix calculations described in the text. Estimated error margins in the last decimal place are given in parentheses. The numerical results are indicated by "(num)." For comparison, we include theoretical values.

n	c (num)	c (exact)	X_m (num)	X_m (exact)
−2.0	−0.99155 (1)	−0.9915599	−0.20179901 (1)	−0.201799000
−1.75	−0.91099 (1)	−0.9109986	−0.17697229 (2)	−0.176972272
−1.50	−0.81973 (1)	−0.8197365	−0.15164470 (2)	−0.151644706
−1.25	−0.71646 (1)	−0.7164556	−0.1259301 (1)	−0.125930086
−1.00	−0.59999 (1)	−6/10	−0.100000000(1)	−1/10
−0.75	−0.46962 (1)	−0.4696195	−0.07409548 (2)	−0.074095457
−0.50	−0.32528 (1)	−0.3252829	−0.048531921(1)	−0.048531921
−0.25	−0.16799 (1)	−0.1679953	−0.023691688(1)	−0.023691689
0	0	0	0	0
0.25	0.175264(1)	0.1752630	0.02211104 (1)	0.0221110351
0.50	0.353480(1)	0.3534792	0.042235700(1)	0.0422356998
0.75	0.529949(1)	0.5299489	0.060000362(1)	0.0600003616
1.00	0.700000(1)	7/10	0.07500000 (1)	3/40
1.25	0.85897 (1)	0.8589769	0.086505216(2)	0.0865052157
1.50	1.00000 (1)	1	0.08801923 (5)	0.0880192310

quence of length u. This sequence can be coded by means of an integer $\sigma(j_1,j_2,\ldots,j_u)$ in the range $1 \leqslant \sigma \leqslant a_u$. The actual values of σ and of a_u are given in Ref. [7]. Let

$$A(\beta) = \Sigma_{\alpha=1}^{\beta-1} a_{u(\alpha)}$$

be the number of connectivities whose binary vacancy number is smaller than β, where $u(\alpha)$ is the number of dangling edges which are not adjacent to a vacant face in the face configuration α. Then, the integer that codes the connectivity with vacancies is

$$\gamma(i_1,i_2,\ldots,i_L) = A(\beta) + \sigma(j_1,j_2,\ldots,j_u). \tag{36}$$

A decoding algorithm, that constructs a sequence $(i_1,i_2,\ldots,i_L)$ given the integer γ, was constructed using similar methods.

B. Numerical calculations

Several eigenvalues of translationally invariant (zero-momentum) eigenstates of the transfer matrix were computed for a limited range of system sizes $L \leqslant 16$ as follows.

(i) The largest eigenvalue $\Lambda_L^{(0)}$ in the "even sector," which means that the transfer matrix operates in the space of connectivities whose dangling bonds occur only in connected pairs.

(ii) The second largest eigenvalue $\Lambda_L^{(1)}$ in the same sector.

(iii) The largest eigenvalue $\Lambda_L^{(2)}$ in the "odd sector," which means that the transfer matrix operates in the space of connectivities with, apart from dangling pairs of bonds, precisely one dangling bond that is single.

(iv) The largest eigenvalue $\Lambda_L^{(3)}$ in the even sector of the transfer matrix of a model with a "seam." The seam modifies one row of bonds. These bonds are perpendicular to the axis, while the row itself is parallel to the axis. All edges of this seam contribute a factor of −1 to the Boltzmann weight, if covered by a loop segment. In actual calculations, this is realized by changing the sign of some of the vertex weights of Fig. 2 and Eq. (22), for those vertices that are immediately to the left of the seam.

The finite-size data for the largest eigenvalue $\Lambda_L^{(0)}$ determine the free energy density, from which we estimated the conformal anomaly c [18,19]. The ratio $\Lambda_L^{(1)}/\Lambda_L^{(0)}$ defines the correlation length of the energy-energy correlation function. Using Cardy's conformal mapping [23] of an infinite cylinder on the infinite plane, one can thus estimate the temperature dimension X_t. Similarly, $\Lambda_L^{(2)}/\Lambda_L^{(0)}$ is used to find the magnetic dimension X_h. Finally the ratio $\Lambda_L^{(3)}/\Lambda_L^{(0)}$ yields the so-called interface exponent X_{int}. All of the quantities c, X_t, X_h, and X_{int} were already described exactly as a function of n and verified numerically; see Ref. [8] and references therein. The present numerical analysis is aimed at confirming that the present model describes the tricritical O(n) model. The numerical analysis follows basically the lines of Refs. [7,15]; see also [24]. The final estimates are listed in Tables I and II. They agree convincingly with the analytic expressions listed in Sec. IV whose values are also included in the tables.

VI. DISCUSSION

The present tricritical O(n) model appears to belong to the same universality class as a loop model defined in Ref. [9]. The latter model was defined as the surrounding loop model of the critical q-state random cluster model on the square lattice. It is possible to apply the same method as used above—namely, to use the ADE interpretation and to restore the loops except those surrounding the vacancies of type a and d—to the latter loop model. We have chosen the present formulation based on the low-temperature O(n) model of

TABLE II. Temperature critical dimension X_t and magnetic dimension X_h as determined from the transfer-matrix calculations described in the text. Estimated error margins in the last decimal place are given in parentheses. The numerical results are indicated by "(num)." For comparison, we include theoretical values.

n	X_t (num)	X_t (exact)	X_h (num)	X_h (exact)
−2.0			−0.0951628 (1)	−0.0951627339
−1.50		0.709784688	−0.0876432 (1)	−0.0876431495
−1.25	0.4814737 (2)	0.481473928	−0.0790909 (1)	−0.0790908776
−1.00	0.39999999 (1)	2/5	−0.05833333 (1)	−7/120
−0.75	0.3446680 (2)	0.344668096	−0.045889544(1)	−0.0458895426
−0.50	0.3039307 (2)	0.303930873	−0.031982842(2)	−0.0319828413
0.00	0.2500000 (1)	1/4	0	0
0.25	0.2324956 (1)	0.232495729	0.017729518(1)	0.0177295181
0.50	0.2192386 (1)	0.219238626	0.03627658 (1)	0.0362765827
0.75	0.2088742 (1)	0.208874121	0.05539746 (1)	0.0553974632
1.00	0.20000001 (1)	1/5	0.07500000 (1)	3/40
1.25	0.19068002 (1)	0.190680043	0.09549715 (1)	0.0954971419
1.50	0.16844985 (5)	0.168449854	0.125000000(1)	1/8

branch 2 defined in Refs. [6,7]. This is more natural in the sense that it allows for sites that are neither visited by a loop nor adjacent to a vacancy. The relations between the various models, as constructed and listed in Secs. II and III, are summarized by

$$Z_{\text{spin}} \leftrightarrow Z_{\text{dense loop}} \leftrightarrow Z_{\text{ADE}} \leftrightarrow Z_{\text{loop+vac}} \leftrightarrow Z_{\text{dilute spin}}. \tag{37}$$

The last step follows from the general equivalence formulated in Sec. II.

As found in Ref. [8], the introduction of vacant faces in the honeycomb O(n) model leads to tricriticality when the fugacity of the vacancies is sufficiently large. No vacancy-vacancy couplings were introduced. Numerical work on the square lattice O(n) model for $n=1$ revealed a peculiar difference with the honeycomb O(n) model. No tricritical point was found when vacancy-vacancy couplings are absent. Instead, a multicritical point resembling that of branch 3 of Ref. [7] was found. The physical interpretation of this multicritical point is that the O(n) critical line merges with an Ising critical line, where auxiliary variables in the form of dual Ising spins undergo a phase transition. A qualitative difference with the model described by the vertex weights of Eq. (22) is that the vacancies attract each other in the latter model.

A comparison of the numerical results for the present model with those for the tricritical honeycomb model O(n) studied in Ref. [8] shows a conspicuous difference in the estimated accuracies. This difference can be explained from the way in which the two different sets of tricritical points were found. For the honeycomb lattice O(n) model of Ref. [8], the tricritical points were determined numerically in a small parameter space. From the perspective of the renormalization theory, this procedure yields a rather arbitrary tricritical point in the sense that the irrelevant fields are nonzero in general and thus introduces corrections to scaling. In contrast, the exact equivalence of the present tricritical square-lattice O(n) model with the O(n) low-temperature branch indicates that the leading irrelevant field vanishes, since the equivalent O(n) low-temperature branch is characterized by the vanishing of its irrelevant temperature field. As a result, the corrections to scaling are suppressed and the apparent finite-size convergence improves drastically.

Since it is widely believed that the universal parameters describing the critical state are determined by the symmetry of the model, the dimensionality, and the range of interaction, it seems plausible that the tricritical model presented above serves as a representative of the generic O(n) universality in two dimensions. Indeed the spin-spin interactions defined in Sec. II contain only scalar products, which satisfy the O(n) symmetry.

However, in this case the O(n) symmetry of the spin model is not a secure guide for the universality class. This is because, like in the dense loop phase of the pure O(n) model, intersections are relevant [3,5]. The same applies to the tricritical point reported here: the exponent associated with crossing loops is the same as that of cubic symmetry breaking. Recently, Jacobsen *et al.* [4] proposed that the low-temperature phase of the generic O(n) model is described by the intersecting loop model proposed in [25] and since called the Brauer model [26].

It is interesting to note that the mappings described in Sec. III can also be applied to the critical "branch 1" [6,7,11] of the square-lattice O(n) model. Just as branch 1 is the analytic continuation of branch 2, we can continue the tricritical branch through the "end point" $n=3/2$, $g=1$ to $g>1$. The weights for branch 1 are also given by Eq. (5), but instead with $\pi/2<\theta<\pi$. The relation between n and n' remains the same, but the vertex weights as specified by Eq. (5) change, and the relation between the Coulomb gas coupling and the conformal classification parameter m is no longer $g=m/(m+1)$, but becomes $g=(m+1)/m\geqslant 1$, while it relates to n' as $n'=2\cos(\pi/m)$ (see, e.g., Ref. [7]). For $n=1$ or $n'=(1+\sqrt{5})/2$ one thus finds a higher critical Ising

model that is to be compared with the $m=5$ model in the series of Andrews *et al.* [27]. For $n=0$ or $n'=1$ the model displays an Ising-like critical point. The resulting branch of multicritical points can thus be seen as a generalization of the $m=5$ Ising-like model for $n=1$ to continuous values of n—i.e., the point where the tricritical point itself turns first-order.

ACKNOWLEDGMENTS

This research is supported by the NSFC under Grant No. 10675021, by the Beijing Normal University through a grant as well as support from its HSCC (High Performance Scientific Computing Center), and, in part, by the Lorentz Fund. We thank Youjin Deng for some valuable discussions.

[1] H. E. Stanley, Phys. Rev. Lett. **20**, 589 (1968).
[2] E. Domany, D. Mukamel, B. Nienhuis, and A. Schwimmer, Nucl. Phys. B **190**, [FS3], 279 (1981).
[3] B. Nienhuis, Phys. Rev. Lett. **49**, 1062 (1982); J. Stat. Phys. **34**, 731 (1984).
[4] J. L. Jacobsen, N. Read, and H. Saleur, Phys. Rev. Lett. **90**, 090601 (2003).
[5] B. Nienhuis, in *Phase Transitions and Critical Phenomena*, edited by C. Domb and J. L. Lebowitz (Academic Press, London, 1987), Vol. 11.
[6] M. T. Batchelor, B. Nienhuis, and S. O. Warnaar, Phys. Rev. Lett. **62**, 2425 (1989).
[7] H. W. J. Blöte and B. Nienhuis, J. Phys. A **22**, 1415 (1989); B. Nienhuis, Int. J. Mod. Phys. B **4**, 929 (1990).
[8] W.-A. Guo, B. Nienhuis, and H. W. J. Blöte, Phys. Rev. Lett. **96**, 045704 (2006).
[9] B. Nienhuis, S. O. Warnaar, and H. W. J. Blöte, J. Phys. A **26**, 477 (1993).
[10] Y. M. M. Knops, H. W. J. Blöte, and B. Nienhuis, J. Phys. A **26**, 495 (1993).
[11] S. O. Warnaar, P. A. Pearce, K. A. Seaton, and B. Nienhuis, J. Stat. Phys. **74**, 469 (1994).
[12] V. Pasquier, J. Phys. A **20**, L1229 (1987).
[13] V. Pasquier, Nucl. Phys. B **285** [FS19], 162 (1987).
[14] V. Pasquier, J. Phys. A **20**, 5707 (1987).
[15] H. W. J. Blöte and M. P. Nightingale, Physica A **112**, 405 (1982).
[16] R. J. Baxter, J. Phys. A **19**, 2821 (1986); **20**, 5241 (1987).
[17] M. T. Batchelor and H. W. J. Blöte, Phys. Rev. Lett. **61**, 138 (1988); Phys. Rev. B **39**, 2391 (1989).
[18] H. W. J. Blöte, J. L. Cardy, and M. P. Nightingale, Phys. Rev. Lett. **56**, 742 (1986).
[19] I. Affleck, Phys. Rev. Lett. **56**, 746 (1986).
[20] W. Janke and A. M. J. Schakel, Phys. Rev. Lett. **95**, 135702 (2005).
[21] Y. Deng, T. M. Garoni, W.-A. Guo, H. W. J. Blöte, and A. D. Sokal, Phys. Rev. Lett. **98**, 120601 (2007).
[22] B. Duplantier and H. Saleur, Phys. Rev. Lett. **59**, 539 (1987).
[23] J. L. Cardy, J. Phys. A **17**, L385 (1984).
[24] For reviews, see, e.g., M. P. Nightingale, in *Finite-Size Scaling and Numerical Simulation of Statistical Systems*, edited by V. Privman (World Scientific, Singapore 1990); M. N. Barber, in *Phase Transitions and Critical Phenomena*, edited by C. Domb and J. L. Lebowitz (Academic, New York 1983), Vol. 8.
[25] M. J. Martins, B. Nienhuis, and R. Rietman, Phys. Rev. Lett. **81**, 504 (1998); M. J. Martins and B. Nienhuis, J. Phys. A **31**, L723 (1998).
[26] J. de Gier and B. Nienhuis, J. Stat. Mech.: Theory Exp. (2005) P01006.
[27] G. E. Andrews, R. J. Baxter, and P. J. Forrester, J. Stat. Phys. **35**, 193 (1984).